JHEP|Reports

# Artificial intelligence as a ploy to delve into the intricate link between genetics and mitochondria in patients with MASLD


## Authors

Miriam Longo, Erika Paolini, Marica Meroni, …, Maurizio Moggio, Anna Ludovica Fracanzani, Paola Dongiovanni

## Correspondence

paola.dongiovanni@policlinico.mi.it (P. Dongiovanni).


## Graphical abstract

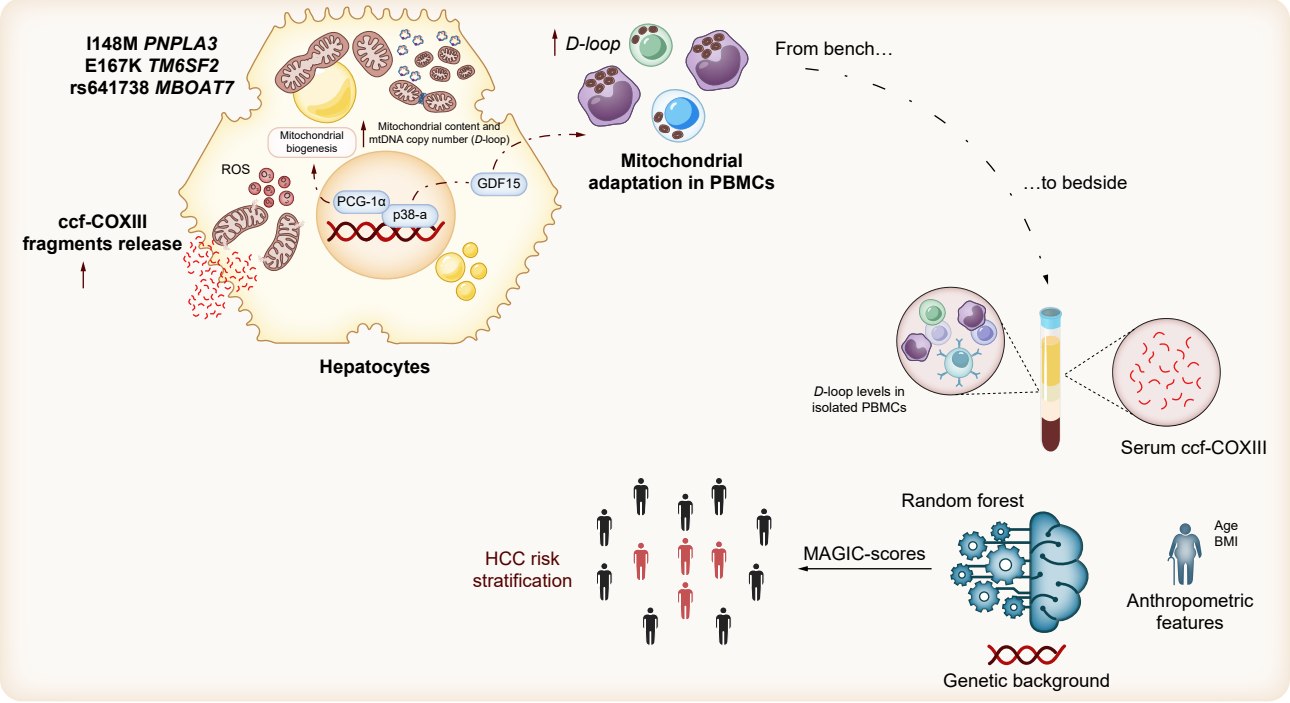


## Highlights:

- The cumulative presence of *PNPLA3*, *MBOAT7*, and *TM6SF2* variants alter hepatic mitochondrial dynamics in patients with MASLD.
- Circulating mitochondrial biomarkers reflect the hepatic mitochondrial changes and correlate with SNPs and MASLD severity.
- Circulating mitochondrial biomarkers and polygenic risk scores alone did not improve clinical risk stratification of patients with MASLD.
- Machine-learning analysis aids in the development of efficacious prediction models for MASH, fibrosis and HCC.

## Impact and implications:

The study highlights that genetic variants in *PNPLA3*, *MBOAT7*, and *TM6SF2* genes deeply contribute to metabolic dysfunction-associated steatotic liver disease (MASLD) progression by affecting hepatic mitochondrial adaptability. It also identified two novel biomarkers of mitochondrial origin which are strongly linked to disease severity and genetic background of patients with MASLD. The use of generative artificial intelligence tools, such as GPT-4, can enhance the use of biomarkers and polygenic risk scores for clinical risk stratification. We developed a customized version of GPT-4 (rsGPT-4), which identified a machine-learning approach (random forest) as the best method for creating prediction models for metabolic dysfunction-associated steatohepatitis, fibrosis, and hepatocellular carcinoma. The new scores combined the two mitochondrial biomarkers, genetic data, and anthropometric data and outperformed existing non-invasive tests for monitoring patients with MASLD.

https://doi.org/10.1016/j.jhepr.2025.101539

 

Research article

JHEP|Reports

# Artificial intelligence as a ploy to delve into the intricate link between genetics and mitochondria in patients with MASLD

Miriam Longo[1], Erika Paolini[1], Marica Meroni[1], Michela Ripolone[2], Laura Napoli[2], Francesco Gentile[3], Annalisa Cespiati[1,4], Elena Trombetta[5], Rosa Lombardi[1,4], Marco Maggioni[6], Anna Alisi[7], Luca Miele[8,9], Antonio Liguori[8], Giorgio Soardo[10], Antonio Gasbarrini[8,9], Maurizio Moggio[2], Anna Ludovica Fracanzani[1,4], Paola Dongiovanni[1,*]

JHEP Reports **2025**. vol. 7 | 1–13



**Background & aims:** Mitochondrial (mt-) *D-loop* and cell-free circulating (ccf-) mtDNA fragments, respectively reflecting mt-mass and tissue damage, are promising metabolic dysfunction-associated steatotic liver disease (MASLD) biomarkers. We previously found that *PNPLA3/MBOAT7/TM6SF2* deficiency in HepG2 cells increased mt-mass, *D-loop* levels, and ccf-COXIII release. We explored mt-biogenesis and mt-biomarkers in patients with MASLD stratified by the number of risk variants (NRV = 3). We exploited GPT-4 to develop and validate new risk scores, predicting MASLD evolution, in two independent cohorts by integrating anthropometric and genetic data with mt-biomarkers.

**Methods:** A cohort of 28 patients with MASLD (Discovery cohort) was consecutively enrolled for hepatic mt-dynamics assessment by transmission electron microscopy and immunohistochemistry. Data were confirmed by quantitative real time-PCR in a retrospective cohort (Hepatic Validation, n = 184). *D-loop* and ccf-COXIII were retrospectively measured in peripheral blood mononuclear cells and serum samples of biopsied outpatients with MASLD (Serum Validation cohort, n = 824) and individuals with non-invasive MASLD diagnosis (n = 386, Non-invasive cohort). Risk scores were developed using random forest algorithms.

**Results:** In the Discovery and Hepatic Validation cohorts, the *PNPLA3/MBOAT7/TM6SF2* variants altered hepatic mt-dynamics, enhancing mt-content and *D-loop* levels ($p$ <0.05) through the p38/PGC-1α pathway. Furthermore, NRV = 3 patients showed an increase in mt-fragmentation at transmission electron microscopy (TEM) and ccf-COXIII release ($p$ <0.05). In the Serum Validation cohort, circulating *D-loop* and ccf-COXIII positively correlated with genetics [$\beta_{D\text{-}loop}$:0.17 (95% CI: 0.04–0.29), $p$ = 0.01; $\beta_{ccf\text{-}COXIII}$:0.33 (95% CI: 0.19–0.46), $p$ <0.0001] and MASLD severity [$OR_{D\text{-}loop}$:1.31 (95% CI: 1.01-1.71), $p$ = 0.03; $OR_{ccf\text{-}COXIII}$:2.41 (95% CI: 1.69-3.44), $p$ <0.0001] at multivariate analysis. Random forest allowed prediction models named Mitochondrial, Anthropometric, and Genetic Integration with Computational intelligence for assessing hepatocellular carcinoma risk (MAGIC-H), considering age, BMI genetics, *D-loop*, and ccf-COXIII. In both Serum and Non-invasive cohorts, the MAGIC-H score reached AUC >85% in identifying HCC cases regardless of cirrhosis, outperforming existing non-invasive tests.

**Conclusions:** Mt-biomarkers have a prognostic significance in genetically-predisposed patients with MASLD.



## Introduction

Metabolic dysfunction-associated steatotic liver disease (MASLD) spans from MASL to metabolic dysfunction-associated steatohepatitis (MASH), fibrosis, and hepatocellular carcinoma (HCC).[1] *PNPLA3*, *MBOAT7*, and *TM6SF2* missense single nucleotide polymorphisms (SNPs), regulating lipid metabolism, are the major MASLD genetic predictors and their cumulative presence increases the risk to progress up to HCC.[2–4]

Mitochondria (mt-) are dynamic organelles with balanced fusion, fission, and mitophagy events. During MASLD progression, mt-dynamics is lost, leading to the formation of dysfunctional and misshaped mitochondria.[5–7] Although the role of mt-dysfunction in disease progression is well established, the impact of genetics on mt-dynamics in MASLD has been poorly described. Recently, we demonstrated that *PNPLA3/MBOAT7/TM6SF2* haploinsufficiency impairs mt-biogenesis in hepatocytes through *peroxisome proliferator-activated receptor-gamma coactivator (PGC)-1α*, one of the major regulators of mt-dynamics, causing accumulation of defective mitochondria and metabolic reprogramming.[8]

Several studies underlined the urgent need to develop MASLD risk predictive models attempting to monitor disease progression without recurring liver biopsy. The evaluation of the *D-loop* region, involved in mtDNA replication, and cell-free circulating mtDNA (ccf-mtDNA) are gaining attention for

* Corresponding author. Medicine and Metabolic Diseases, Fondazione IRCCS Cà Granda Ospedale Maggiore Policlinico, Milan, Italy, via Pace 9, 20122, Milano, MI, Italy. Tel.: +39 02 5503 3467; fax: +39 02 5503 4229.
*E-mail address:* paola.dongiovanni@policlinico.mi.it (P. Dongiovanni).
https://doi.org/10.1016/j.jhepr.2025.101539

MASLD non-invasive assessment.[9] The *D-loop* may reflect mt-content/dynamics, whereas the release of ccf-mtDNA components (*i.e.* ccf-COXIII), consequent to mt-damage, may worsen tissue inflammation and fibrosis.[10,11] Furthermore, the efforts for the development of reliable risk scores to apply in clinical practice are limited by the observed low accuracy rates.[2,12] Nonetheless, the advent of artificial intelligence (AI) and its current applications in healthcare may pave the way for big data mining, thus allowing researchers to apply AI in different fields, from medical imaging to clinical data analysis.

The central hypothesis of this work was to provide proof that a link between *PNPLA3*, *MBOAT7*, and *TM6SF2* genetic variants and mt-turnover exist in patients with MASLD. For this purpose, we first assessed hepatic mt-dynamics in a newly and consecutively enrolled cohort of 28 patients undergoing liver biopsy for clinical indications (Discovery cohort), who were stratified according to the number of risk variants (NRV).[8] Liver biopsies underwent transmission electron microscopy (TEM) and immunohistochemistry (IHC) analysis for the evaluation of mt-morphology and mt-dynamics markers, respectively. Then, mt-biogenesis was further investigated in 184 liver biopsies (Hepatic Validation cohort). Secondly, we aimed to identify novel biomarkers which may reflect the hepatic mt-alterations, thus providing new approaches for clinical risk assessment. Thus, we assessed whether circulating *D-loop* and ccf-COXIII were further associated with MASLD-related genetic background and whether their evaluation may be indicative of changes in hepatic mt-dynamics and tissue damage, respectively, in 824 biopsied patients with MASLD (Serum Validation cohort). Finally, we took advantage of GPT-4 to develop predictive non-invasive scores, including anthropometric, genetic data, and mt-biomarkers, testing them as potential diagnostic/prognostic tools for identification of both early and late-stages of MASLD. The new models were first trained in the Serum Validation cohort and then applied in an independent cohort of patients, who underwent elastography ultrasound (FibroScan®, Echosens, Paris, France) for MASLD assessment (n = 386, Non-invasive cohort). AI-guided prediction models were compared with existing non-invasive tests (NITs) and an AI-guided score generated with transaminases.

## Materials and methods

### Human samples, mt-biomarkers measurements, and GPT-4

All studies with human material were approved by the Ethical Committee at Fondazione IRCCS Cà Granda, Ospedale Maggiore Policlinico Milano and conformed to the 1975 Declaration of Helsinki. Hepatic mt-morphology, content, and ultrastructural defects were assessed using TEM, whereas hepatic expression and localization of mt-dynamics markers were assessed using IHC.

For measuring *D-loop* and ccf-COXIII levels, mtDNA was extracted from peripheral blood mononuclear cells (PBMCs) and serum samples, respectively, using a QIAmp DNA Mini Kit (QIAGEN, Manchester, UK). The *D-loop* region was amplified through the TaqMan Copy Number Assay (MT-7S, ThermoFisher, Waltham, USA, #Hs02596861_s1). RNAse-P (ThermoFisher #4401631), a sequence known to exist in two copies in the human genome, was used as a reference gene. For ccf-COXIII, the following primers were designed: forward 5′-TGACCCACCAATCACATGC-3′ and reverse 5′-ATCA-CATGGCTAGGCCGGAG-3′.

The OpenAI GPT-4 language model was exploited for the construction of risk scores for MASLD diagnosis and/or progression. Stringent anonymization measures were applied to the dataset before analysis, removing all direct personal identifiers to safeguard patient confidentiality and adhere to privacy regulations. We used a customized GPT-4 environment through GPT-builder, specifically enhanced for advanced coding, statistical analysis, and processing large datasets (labeled as risk score GPT-4, rsGPT-4). rsGPT-4 identified key columns corresponding to age, BMI, NRV, *D-loop*, and ccf-COXIII, as essential parameters of interest. All methodological details are described in the Supplementary material.

## Results

### *PNPLA3*/*MBOAT7*/*TM6SF2* SNPs exacerbate alterations of mt-morphology and content in the discovery cohort

A case series of 28 newly enrolled biopsied patients with MASLD (Discovery cohort, Table S1) was included in the study to explore mt-morphological changes and mt-dynamics by TEM and IHC, respectively, according to both disease severity (Fig. S1A–D) and genetic background.

Patients' genotyping identified only one non-carrier (NRV = 0), 11 carriers of one at-risk variant (NRV = 1), 12 carriers of two mutations (NRV = 2), and four (NRV = 3) carrying all the three SNPs, further showing the highest Non-alcoholic fatty liver disease Activity Score (NAS) and fibrosis grade (NAS = 6–7: 100% NRV = 3 *vs.* 42% *vs.* NRV = 0–1–2; F2–3: 75% NRV = 3 *vs.* 39.5% NRV = 0–1–2), thus supporting that prevalence of disease severity progressively increases as the NRV.[8]

At TEM, NRV = 3 patients displayed the highest mt-number ($p = 0.002$ at ANOVA; adj $p < 0.05$ *vs.* NRV = 0–1–2; Fig. 1A–D). At the generalized linear model (GLM), the hepatic mt-content inferred from TEM images, was associated with NRV = 3, independently of MASLD severity (Table 1), thus suggesting a potential contribution of genetic background to the modulation of mt-biogenesis.

Furthermore, NRV = 3 patients presented the largest mt-size compared with those with NRV = 0–1–2 (perimeter: $p = 0.009$ at ANOVA; adj $p < 0.05$ *vs.* NRV = 0–1–2; area: $p = 0.02$ at ANOVA; adj $p < 0.05$ *vs.* NRV = 0–1–2; Fig. 1C–D). NRV = 3 carriers accumulated a wide array of mt-morphological alterations including canonical defects (paracrystalline inclusions, giant mitochondria, GM), shared among individuals with a moderate/severe NAS (Fig. S1A–D) and new ones as: (a) rupture of mt-double membranes; (b) abnormal distribution of the internal cristae (round-shaped; flattened sideways); (c) swollen mitochondria with loss of internal matrix; (d) irregular mt-morphology (three-branched); and (e) vacuoles inside rounded mitochondria (Fig. 1E).

These results suggest that NRV = 3 carriers not only increase mt-mass but further show a wider spectrum of mt-ultrastructural lesions.

### *PNPLA3*/*MBOAT7*/*TM6SF2* SNPs associate with hepatic impairment of mt-dynamics in the discovery cohort

To validate our hypothesis, we explored the hepatic expression of PGC-1α and downstream mediators regulating mt-biogenesis and turnover by IHC.

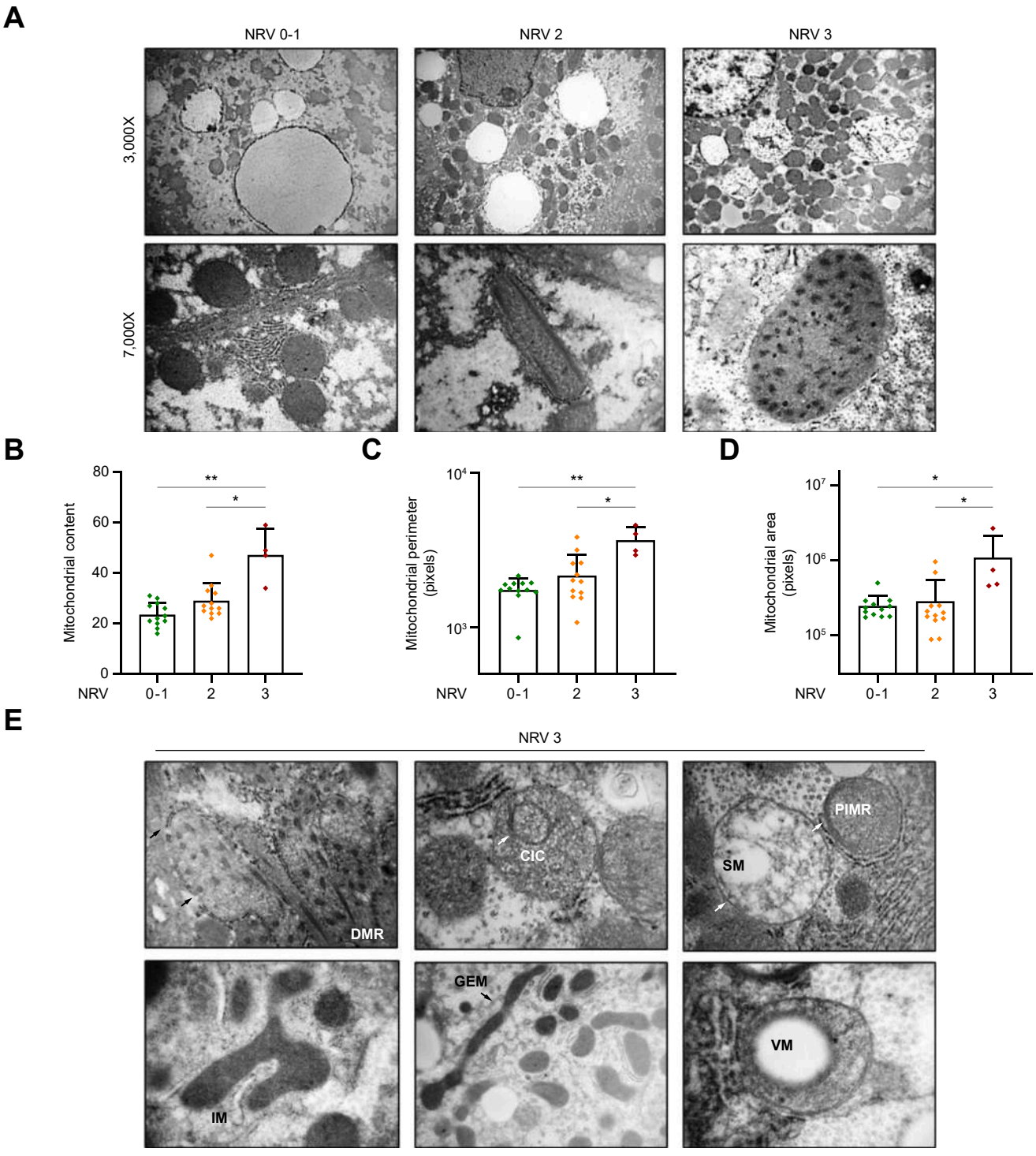


**Fig. 1. The effects of *PNPLA3*/*MBOAT7*/*TM6SF2* SNPs on mt-morphology in the Discovery cohort.** (A) Representative TEM images showing mt-mass (on top, 3,000 × magnification) and canonical mt-defects as PIs and GMs (on bottom; 7,000 × magnification) in patients with MASLD stratified according to NRV. (B–D) Bar graphs show the quantification of the mt-number ($p$ = 0.002 at ANOVA; adj $p$ = 0.001 NRV = 3 *vs.* NRV = 0–1; adj $p$ = 0.03 NRV = 3 *vs.* NRV = 2), mt-perimeter ($p$ = 0.009 at ANOVA; adj $p$ = 0.004 NRV = 3 *vs.* NRV = 0–1; adj $p$ = 0.03 NRV = 3 *vs.* NRV = 2), and mt-area ($p$ = 0.02 at ANOVA; adj $p$ = 0.02 NRV = 3 *vs.* NRV = 0–1; adj $p$ = 0.01 NRV = 3 *vs.* NRV = 2), through ImageJ in a range of six random images per patient. (E) Non-canonical mt-morphological damages in NRV = 3 patients with MASLD included: DBR (double-membrane rupture); CIC (circular internal cristae); SM (swollen mitochondria); PIMR (packed internal membranes rearrangements); GEM (giant elongated mitochondria); IM (irregular morphology); and VM (vacuolated mitochondria). Differences between groups were calculated by one-way nonparametric ANOVA (Kruskal–Wallis), followed by Dunn's multiple comparison adjustment. mt-, mitochondria; MASLD, metabolic dysfunction-associated steatotic liver disease; NRV, number of risk variants; SNPs, single nucleotide polymorphisms; TEM, transmission electron microscopy.

**Table 1. GLM correlating hepatic mt-content and circulating *D-loop* with NAS≥5 and presence of NRV = 3 variants in the Discovery cohort (n = 28).**

| | Hepatic mitochondrial content | | Circulating *D-loop* | |
|---|---|---|---|---|
| | β (95% CI) | *p* value | β (95% CI) | *p* value |
| Age, years | -0.19 (-0.54 to 0.15) | 0.25 | -0.03 (-0.08 to 0.02) | 0.19 |
| BMI, kg/m$^2$ | -0.26 (-0.97 to 0.44) | 0.44 | -0.02 (-0.11 to 0.07) | 0.67 |
| NAS (*vs.* Mild) | | | | |
| Moderate <5 | -3.04 (-7.92 to 1.83) | 0.21 | 0.39 (-0.28 to 1.06) | 0.24 |
| Severe ≥5 | 7.99 (3.98 to 11.99) | **0.0003** | 0.08 (-0.47 to 0.64) | 0.73 |
| NRV = 3 | 7.18 (3.37 to 10.99) | **0.0006** | 0.61 (0.08 to 1.14) | **0.02** |

Values are reported as mean ± SD, n (%), or median (IQR), as appropriate. GLM was adjusted for age, BMI, NAS, and NRV. Variables with skewed distribution (*D-loop*) were logarithmically transformed before analyses. *p* <0.05 was considered statistically significant in bold. GLM, generalized linear model; mt-, mitochondria; NAS, Non-alcoholic fatty liver disease Activity Score; NRV, number of risk variants.

PGC-1α was highly expressed in the hepatic parenchyma of NRV = 3 patients with MASLD. NRV = 0–1 patients showed ~20% of nuclear PGC-1α expression, and the amount of positive cells increases of ~40% and 80% in NRV = 2 and NRV = 3 patients, respectively (*p* = 0.001 at ANOVA; adj *p* <0.05 NRV = 3 *vs.* NRV = 0–1–2; adj *p* <0.05 NRV = 2 *vs.* NRV = 0–1, Fig. 2, Table S2), thus supporting that its transcriptional activity proportionally increases as the NRV.

To give strength to our data, we labeled mitochondria with a specific antibody recognizing mt-surface and investigated the protein expression of key PGC-1α cofactors (Fig. 2). We looked at the canonical SIRT1/AMPK signaling and alternative pathways related to oxidative stress and proliferation (mTORC1, ERK/JNK/p38), which may potentially explain the hepatic PGC-1α increase.[13,14] Mt-content significantly raised in NRV = 3 patients (*p* = 0.01 at ANOVA; adj *p* <0.05; NRV = 3 *vs.* NRV = 0–1; Table 1), forming large spotty marks near the lipid droplets (LDs). Lower phospho(T172)-AMPK activation was found in NRV = 3 patients compared with non-carriers and NRV = 1–2 individuals, thus supporting an impairment of the SIRT1/AMPK signaling.[13] None of the three groups showed phospho(Ser2448)-mTOR signals in liver biopsies. Conversely, a broader cytoplasmatic positivity for phospho (T202/Y204)-p44/42 MAPK (phospho-ERK) and phospho (T183/Y185)-JNK along with nuclear phospho(T180/Y182)-p38α activation was detected in NRV = 3 patients compared with NRV = 0–1–2 (Fig. 2). Such observations confirmed the results obtained by TEM, suggesting that hepatic mt-mass increases in NRV = 3 carriers and is likely driven by ERK/JNK/p38 activation.

Mitofusin 1/2 expression, mediating mt-outer membrane aggregation, was unchanged among patients with MASLD (Fig. 3). Conversely, mt-dynamin-like GTPase (OPA1), regulating mt-inner membranes fusion, was markedly increased in NRV = 3 patients, capping around the LDs (*p* = 0.005 at ANOVA; adj *p* <0.05 *vs.* NRV = 0–1–2; Table S2; Fig. 3), thereby indicating that it may play a key role in enhancing mt-fusion, potentially contributing to GM formation.

Dynamin-related protein 1 (DRP1) levels, promoting mt-fission, were higher in NRV = 3 patients compared with non-carriers or carriers of one to two variants (*p* = 0.007 at ANOVA; adj *p* <0.01 *vs.* NRV = 0–1–2; Table S2; Fig. 3) and its expression strongly intensified nearby the LDs.

During mt-fission, mitophagy may be activated to eliminate damaged mitochondria. Therefore, we investigated the expression of PINK1 and its downstream effector, Parkin (PRKN), principal orchestrators of mitophagy.

Although PINK1 was highly expressed in NRV = 3 patients (*p* = 0.0002 at ANOVA, adj *p* <0.01 *vs.* NRV = 0–1, Table S2; Fig. 3), PRKN was markedly reduced (*p* = 0.02 at ANOVA; adj *p* <0.05 *vs.* NRV = 0–1–2; Table S2; Fig. 3), thus suggesting that mitophagy may be early arrested, leading to hepatic mt-accumulation.

Collectively, our data showed that mt-biogenesis is augmented in NRV = 3 carriers, as evidenced by a significant induction of PGC-1α, OPA1, and DRP1, thereby contributing to the observed increase in mt-content. OPA1 and DRP1 proteins, in turn, may facilitate the formation of GM and small, round-shaped mitochondria, respectively. However, our findings have also revealed a plethora of ultrastructural abnormalities among the accumulated mitochondria in NRV = 3 patients. These defects are likely resistant to complete eradication through the PINK1–PRKN pathway, given that the signaling cascade seems to be prematurely halted in these individuals.

### Assessment of systemic mt-biomarkers and hepatic mt-changes across discovery and validation cohorts

We next examined whether hepatic mt-homeostasis changes were mirrored by circulating mt-derived biomarkers (*D-loop* and ccf-COXIII). In the Discovery cohort, circulating *D-loop* correlated positively with the hepatic mt-number quantified by TEM and it was higher in NRV = 3 patients *vs.* NRV = 0–1–2 (Table 1), supporting that these variants impact on mt-content in the liver as in the bloodstream. Similarly, serum ccf-COXIII increased in NRV = 3 patients (Fig. S3A–C), although multivariate analysis did not confirm significance, possibly because of limited power.

Evaluation of mt-biomass in the Hepatic Validation cohort (n = 184) confirmed higher hepatic PGC-1α and *D-loop* in NRV = 3 carriers. A positive correlation among hepatic and circulating *D-loop* levels was also observed in these patients, confirming the results obtained in the Discovery cohort (Fig. S3D–I). To identify potential candidates responsible for the crosstalk between PBMCs and the liver, we analyzed serum levels of growth differentiation factor 15 (GDF15), which is a mitokine released in response to ERK/JNK/p38 pathway activation, in a subset (n = 176) of patients with MASLD belonging to the Serum Validation cohort.[15,16] Serum GDF15 levels were higher in patients with more severe diseases and those with NRV = 3, further correlating with circulating *D-loop* levels (Fig. S3J and L).

### *PNPLA3*/*MBOAT7*/*TM6SF2* variations impact on circulating mt-biomarkers in the Serum Validation cohort

We then measured *D-loop* and ccf-COXIII levels in 824 biopsied patients with MASLD, stratified according to NRV. We

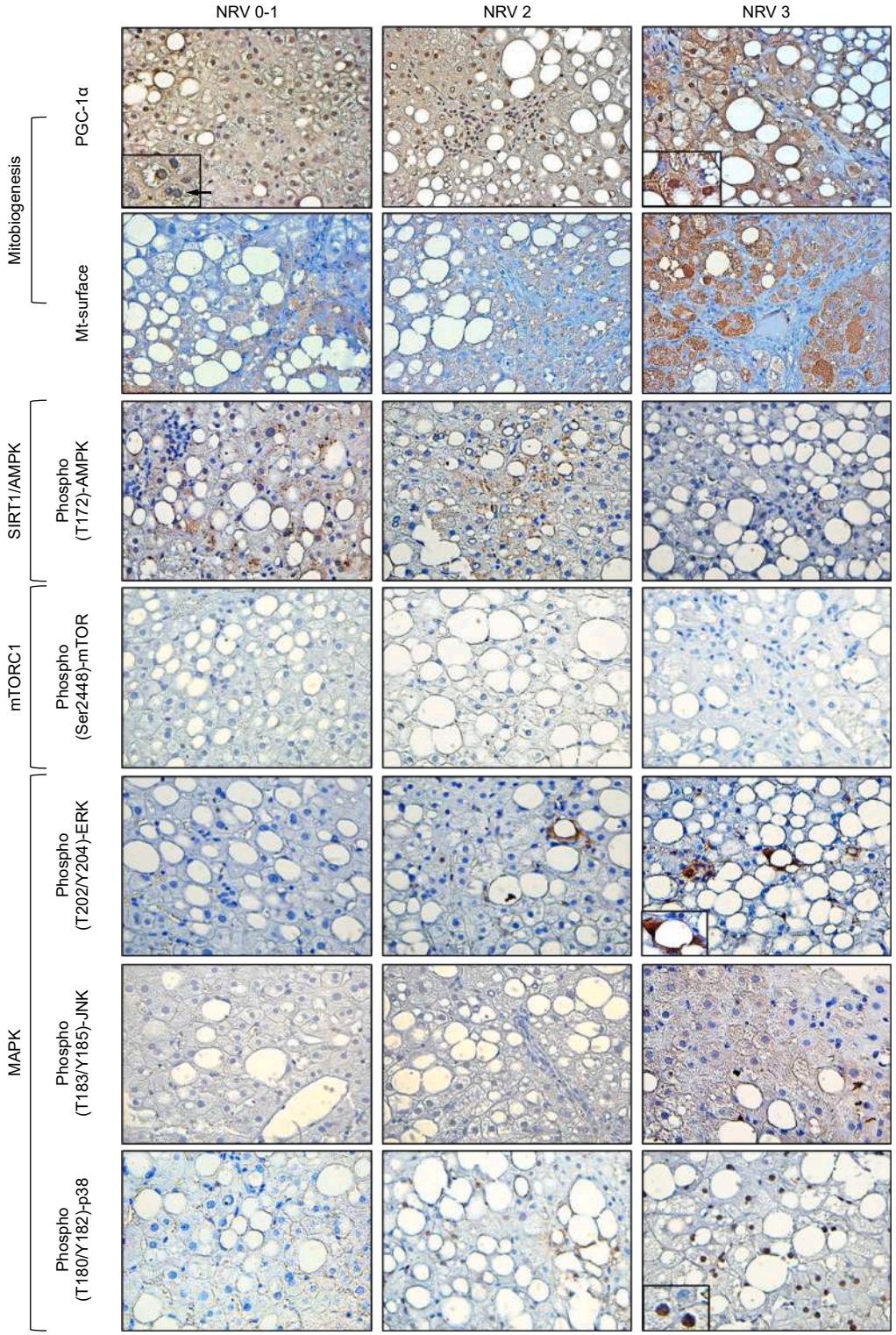


**Fig. 2. *PNPLA3*/*MBOAT7*/*TM6SF2* increases mt-mass in the Discovery cohort.** (A) Representative IHC images showing markers of mt-biogenesis (PGC-1α anti-mitochondrial surface), and upstream signaling pathways (SIRT1/AMPK, mTORC1, MAPK) at 40 × magnification in patients with MASLD stratified according to the NRV. IHC, immunohistochemistry; MASLD, metabolic dysfunction-associated steatotic liver disease; mt-, mitochondria; NRV, number of risk variants; PGC-1α, peroxisome proliferator-activated receptor-gamma coactivator.

revealed that both increase in NRV = 3 carriers at bivariate analysis (*D-loop*: $p = 0.04$ at ANOVA, adj $p < 0.05$ *vs.* NRV = 0–1–2; ccf-COXIII: $p < 0.0001$ at ANOVA, $p < 0.0001$ *vs.* NRV = 0–1–2, Fig. S4A–B) and GLM adjusted for sex, age, BMI and NAS (Table 2), thus supporting a potential role of genetic background in influencing circulating mt-biomarkers.

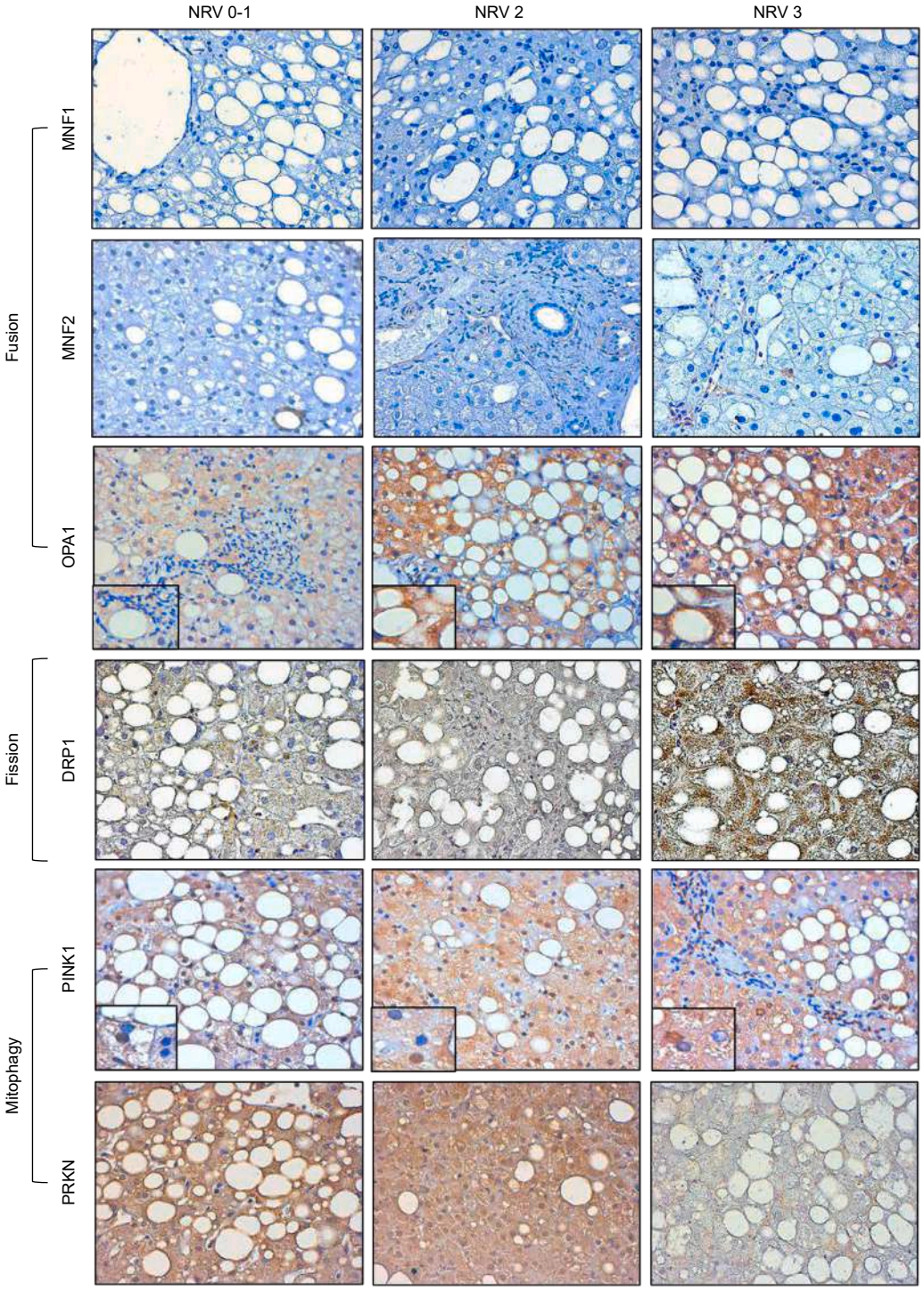


**Fig. 3. Characterization of hepatic mt-biogenesis in NRV = 3 patients from the Discovery cohort.** (A) A representative panel showing the expression of fusion proteins (MFN1/MFN2/OPA1), fission (DRP1) and mitophagy (PINK1, PRKN) assessed by IHC in liver biopsies of patients with MASLD stratified according to NRV (40 × magnification). DRP1, Dynamin-related protein 1; IHC, immunohistochemistry; MASLD, metabolic dysfunction-associated steatotic liver disease; mt-, mitochondria; NRV, number of risk variants; PRKN, Parkin.

We then assessed the individual contribution of PNPLA3 I148M, *MBOAT7* rs641738 C>T, and TM6SF2 E167K mutations in affecting circulating *D-loop* and ccf-COXIII levels. As regards the former, at bivariate analysis, carriers of *MBOAT7* rs641738 C>T or TM6SF2 E167K variants showed elevated *D-loop* expression compared with non-carriers ($p$ = 0.03 at ANOVA; *MBOAT7*: adj $p$ <0.05 CT/TT *vs.* CC; *TM6SF2*: adj $p$ <0.05 CT/TT *vs.* CC, Fig. S4C), whereas no effects were detected with the PNPLA3 I148M SNP. These associations remained significant at the GLM adjusted for confounding

variables (sex, age, BMI, NAS) and the presence of PNPLA3 I148M variant (Table 2), thus indicating that the *PNPLA3* genetic mutation has a lesser impact on circulating *D-loop* levels, compared with *MBOAT7* and *TM6SF2*.

Serum ccf-COXIII increased in carriers of PNPLA3 I148M, *MBOAT7* rs641738 C>T and TM6SF2 E167K SNPs (*p* <0.001 at ANOVA; PNPLA3: adj *p* <0.05 CG/GG *vs.* CC; MBOAT7: adj *p* <0.05 CT/TT *vs.* CC; TM6SF2: adj *p* <0.0001 CT/TT *vs.* CC, Fig. S4D) and correlated with all three single mutations at the GLM adjusted as before (Table 2).

Therefore, data obtained in the Serum Validation cohort highlighted that the three SNPs may affect mt-damage and ccf-COXIII release, but only *MBOAT7* and *TM6SF2* genetic variants seem to play a pivotal role in altering total mt-mass and *D-loop* levels.

### Clinical application of mt-derived biomarkers for the stratification of MASLD at-risk patients

To investigate the potential clinical utility of mt-derived biomarkers, we correlated both circulating *D-loop* and ccf-COXIII levels with anthropometric and histological data of the Serum Validation cohort stratified as follows: MASL, MASH, fibrosis, and MASLD-HCC (Table S1). To assess their disease specificity, we also analyzed circulating *D-loop* and ccf-COXIII in 62 age- and sex-matched healthy individuals, of whom DNA and serum samples were available, and compared their levels with those of patients with MASLD across the cohorts included in the study (Supplementary material).

A positive association between *D-loop* expression and BMI, type 2 diabetes mellitus, Homeostatic Model Assessment for Insulin Resistance, aspartate aminotransferase, lactate, and LDH emerged at GLM, adjusted for confounding factors implicated in disease progression (sex, age, BMI, type 2 diabetes mellitus, and NRV = 3), suggesting that mt-mass changes in response to MASLD-related metabolic comorbidities and indices of liver damage (Table S4).

Accordingly, at bivariate analysis *D-loop* expression progressively increased with disease severity (Table 1) and its levels correlated with severe NAS at GLM (Table 2).

At the ordinal logistic regression analysis corrected as above, *D-loop* was independently associated with the histological degree of steatosis, necroinflammation, ballooning and fibrosis (Table S5). At nominal logistic regression analysis, *D-loop* levels correlated with increased risk of MASH, cirrhosis and MASLD-HCC (Table S6). Taken together, such findings supported that higher *D-loop* levels correlate with environmental factors, genetics and disease severity, thus representing an independent predictor of MASLD progression.

Different from *D-loop*, ccf-COXIII did not correlate with biochemical and anthropometric variables and its serum quantity did not progressively increase across MALSD stages. At GLM, ccf-COXIII showed a trend of correlation with the histological parameters of liver damage and MASH (Tables S5 and S6), but the analysis did not reach statistical significance.

Nonetheless, ccf-COXIII levels were dramatically higher in MASLD-HCC patients compared with those with MASL, MASH, and fibrosis (Table S1). At nominal logistic regression analysis, serum ccf-COXIII showed a significant association with the worst stages of the disease, with an odd ratio of 1.5 and 2.4 for cirrhosis and MASLD-HCC, respectively (Tables S5 and S6). These findings might indicate that the abundance of serum ccf-COXIII fragments observed in individuals with cirrhosis and HCC may reflect the degree of mt-stress and hepatocellular injury, which characterizes late-stage disease, resulting in a promising prognostic measure of advanced MASLD.

### Risk scores development through GPT-4: the role of mt-biomarkers for MASLD-HCC risk

With the outcome to evaluate the clinical efficiency of mt-biomarkers, we developed novel risk scores using a customized rsGPT-4 version (Supplementary material), referred to as

**Table 2. Correlation of D-loop and ccf-COXIII levels with disease severity and SNPs.**

| | Circulating *D-loop* | | Serum ccf-COXIII | |
|---|---|---|---|---|
| | β (95% CI) | *p* value | β (95% CI) | *p* value |
| Sex, M | 0.016 (-0.09 to 0.13) | 0.77 | 0.002 (-0.12 to 0.12) | 0.96 |
| Age, years | 0.004 (-0.003 to 0.01) | 0.21 | 0.001 (-0.007 to 0.009) | 0.79 |
| BMI, kg/m$^2$ | -0.001 (-0.018 to 0.02) | 0.89 | -0.03 (-0.05 to -0.008) | **0.006** |
| NAS (*vs.* Mild) | | | | |
| Moderate <5 | 0.02 (-0.11 to 0.16) | 0.69 | 0.07 (-0.07 to 0.22) | 0.33 |
| Severe ≥5 | 0.24 (0.09 to 0.38) | **0.001** | -0.01 (-0.17 to 0.14) | 0.85 |
| NRV = 3 | 0.17 (0.04 to 0.29) | **0.010** | 0.33 (0.19 to 0.46) | **<0.0001** |
| | **Circulating *D-loop*** | | **Serum ccf-COXIII** | |
| | **β (95% CI)** | ***p* value** | **β (95% CI)** | ***p* value** |
| Sex, M | 0.008 (-0.10 to 0.12) | 0.88 | -0.02 (-0.14 to 0.09) | 0.73 |
| Age, years | 0.004 (-0.003 to 0.01) | 0.27 | -0.0001 (-0.008 to 0.008) | 0.97 |
| BMI, kg/m$^2$ | 0.002 (-0.016 to 0.02) | 0.80 | -0.02 (-0.04 to -0.004) | **0.01** |
| NAS (*vs.* Mild) | | | | |
| Moderate <5 | 0.04 (-0.09 to 0.18) | 0.55 | 0.06 (-0.08 to 0.20) | 0.39 |
| Severe ≥5 | 0.24 (0.09 to 0.38) | **0.001** | 0.05 (-0.04 to 0.10) | 0.50 |
| *PNPLA3* G, yes | 0.03 (-0.09 to 0.18) | 0.55 | 0.11 (0.009 to 0.22) | **0.03** |
| *MBOAT7* T, yes | 0.16 (0.05 to 0.26) | **0.002** | 0.11 (0.003 to 0.21) | **0.04** |
| *TM6SF2* T, yes | 0.12 (0.001 to 0.25) | **0.04** | 0.34 (0.21 to 0.47) | **<0.0001** |

On top, GLM correlates circulating *D-loop* and ccf-COXIII levels, with NAS and NRV = 3 in the Serum Validation cohort (n = 824). On the bottom, GLM correlates both biomarkers with presence and individual *PNPLA3*/*MBOAT7*/*TM6SF2* SNPs. Values are reported as mean ± SD, n (%), or median (IQR), as appropriate. The multivariate was adjusted for sex, age, BMI, NAS, and presence of rs738409 C>G in PNPLA3 (I148M), the rs641738 C>T in MBOAT7 and the rs58542926 C>T in TM6SF2 (E167K) alone or combined (NRV). *p* <0.05 was considered statistically significant. ccf, cell-free circulating; GLM, generalized linear model; NAS, Non-alcoholic fatty liver disease Activity Score; NRV, number of risk variants; SNPs, single nucleotide polymorphisms.

MAGIC (Mitochondrial, Anthropometric, and Genetic Integration with Computational intelligence) for detecting MASH (MAGIC-MASH), fibrosis>1 (MAGIC-Fib), and HCC (MAGIC-H).

After anonymizing the dataset, we asked rsGPT-4 to develop risk scores based solely on non-invasive biomarkers such as *D-loop* and ccf-COXIII, anthropometric, and genetic data (age, BMI, and NRV). Given our dataset characteristics, the AI identified a machine-learning approach (random forest, RF), to obtain high-performance risk scores, which we manually validated on JMP software (SAS Institute Inc., Cary, NC, USA). The RF analyses provided the relative feature importance of the tested parameters and of their interactions, which were subsequently gathered in formulas keeping into account the normalized, importance-weighted predictors. We then applied the risk scores to the Serum Validation cohort, and we generated AUC-ROC curves to determine their prognostic precision on the desired outcomes.

The MAGIC-MASH score built with *D-loop* alone showed a good accuracy (AUC: 73%) for MASH detection, with a discrete balance of sensitivity (65.7%) and specificity (71.3%). Conversely, the AUC of ccf-COXIII was slightly lower at 67%, suggesting it is less discriminative than the *D-loop* for MASH. However, when both biomarkers were combined, the AUC was 69%, showing an increase in sensitivity (73.4%) at the expense of specificity (57.9%). This might suggest that combining these two biomarkers does not necessarily improve the model's ability to discriminate between MASH and non-MASH cases compared with *D-loop* alone (Table 3, Fig. 4A).

As the MAGIC-MASH score with only *D-loop* provided the best performance for assessing the risk of developing MASH, we used it to stratify patients into quartiles as follows: very low-risk (1st quartile: ≤21.65 points), low-risk (2nd quartile: 21.65 to <24.97 points), moderate-risk (3rd quartile: 24.97 to <27.99 points), and high-risk (4th quartile: ≥27.99 points). We observed that patients belonging to the 4th quartile had a significant increased risk of MASH compared with other quartiles (odds ratio [OR] 9.89, 95% CI 5.05–19.37, $p$ <0.0001 *vs.* 1st quartile; OR 7.44, 95% CI 3.66–15.12, $p$ <0.0001 *vs.* 2nd quartile; OR 3.79, 95% CI 1.80–7.97, $p$ = 0.0004 *vs.* 3rd quartile) (Fig. 4B).

When we built the MAGIC-Fib score by considering *D-loop* and ccf-COXIII separately, we observed that *D-loop*, with an AUC of 76%, was again the strongest single biomarker for detecting fibrosis >1 compared with ccf-COXIII (72%). When

**Table 3. AUC-ROC curves comparison performed by MedCalc software, which correlates rsGPT4-based MASLD risk score (MAGIC-) with MASH, fibrosis >1 and HCC risk in the Serum Validation cohort (n = 824).**

| | | | |
|---|---|---|---|
| **MASH, yes** | | | |
| | ***D-loop*** | **Ccf-COXIII** | **Both** |
| AUC | 0.73 | 0.67 | 0.69 |
| 95% CI | 0.69–0.75 | 0.63–0.71 | 0.65–0.73 |
| Z statistics | 11.11 | 6.91 | 7.54 |
| Youden Index J | 0.40 [0.29–0.42] | 0.29 [0.18–0.38] | 0.31 [0.21–0.36] |
| Cut-off | >24.1 | >34.86 | >24.1 |
| Sensitivity (%) | 65.7 | 53.4 | 73.4 |
| Specificity (%) | 71.3 | 75.5 | 57.9 |
| Sample size, n | 824 | 824 | 824 |
| Positive, n (%) | 635 (77) | 613 (74.4) | 626 (77.8) |
| Negative, n (%) | 189 (22.8) | 211 (26.6) | 198 (24) |
| **Fibrosis >1, yes** | | | |
| | ***D-loop*** | **Ccf-COXIII** | **Both** |
| AUC | 0.76 | 0.72 | 0.73 |
| 95% CI | 0.72–0.78 | 0.68–0.75 | 0.69–0.77 |
| Z statistics | 14.28 | 9.59 | 10.34 |
| Youden Index J | 0.41 [0.33–0.4] | 0.35 [0.26–0.40] | 0.38 [0.29–0.44] |
| Cut-off | >26.0 | >36.6 | >30 |
| Sensitivity (%) | 68.0 | 57.4 | 74.0 |
| Specificity (%) | 73.2 | 77.6 | 64.4 |
| Sample size, n | 824 | 824 | 824 |
| Positive, n (%) | 323 (39.2) | 55 (6.7) | 289 (35) |
| Negative, n (%) | 501 (60.8) | 768 (93.3) | 535 (64.9) |
| **HCC, yes** | | | |
| | ***D-loop*** | **Ccf-COXIII** | **Both** |
| AUC | 0.77 | 0.81 | 0.86 |
| 95% CI | 0.74–0.81 | 0.78–0.85 | 0.82–0.88 |
| Z statistics | 14.19 | 9.71 | 17.17 |
| Youden Index J | 0.51 [0.39–0.58] | 0.55 [0.40–0.64] | 0.60 [0.54–0.66] |
| Cut-off | >28.9 | >38.3 | >30 |
| Sensitivity (%) | 73.5 | 75.7 | 78.6 |
| Specificity (%) | 77.5 | 80.1 | 81.5 |
| Sample size, n | 824 | n824 | 824 |
| Positive, n (%) | 92 (11.16) | 55 (6.7) | 44 (5.4) |
| Negative, n (%) | 732 (88.8) | 768 (93.3) | 780 (94.6) |

MAGIC- risk scores aggregated age, BMI, NRV and mt-biomarkers (*D-loop* and/or ccf-COXIII). MAGIC- formulas were achieved by RF analysis. ccf, cell-free circulating; HCC, hepatocellular carcinoma; MASH, metabolic dysfunction-associated steatohepatitis; RF, random forest.

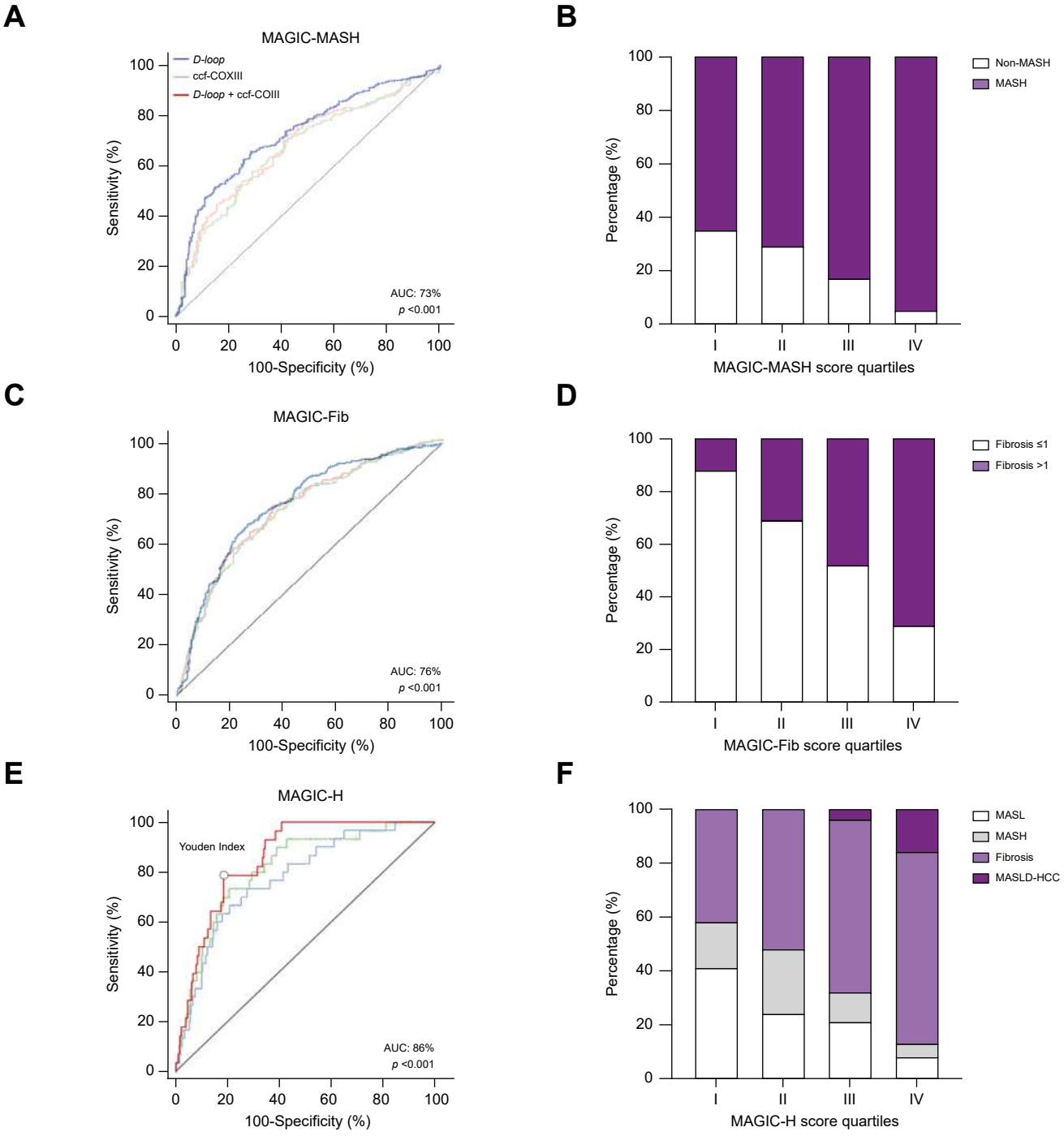


**Fig. 4. Prognostic accuracy of MAGIC risk scores for MASLD clinical assessment, generated through rsGPT-4 guidance, in the Serum Validation cohort.** (A) AUC-ROC curves comparing MAGIC-MASH models generated with mt-biomarkers alone or combined. (B) Contingency analysis displaying the percentage (%) of MASH and non-MASH patients based on MAGIC-MASH quartiles. (C) AUC-ROC curves comparing MAGIC-Fib models built with mt-biomarkers alone or combined. (D) Contingency analysis showing patients with MASLD (%) with fibrosis >1 falling into MAGIC-Fib quartiles. (E) AUC-ROC curves comparing MAGIC-H models developed with mt-biomarkers alone or combined. (F) Contingency analysis shows patients with MASLD (%), with different disease severity, falling into each MAGIC-H quartile. Transparent lines depict alternative scoring models with lesser predictive power, whereas the marked lines highlight the most efficient score identified by the random forest analysis. MAGIC, Mitochondrial, Anthropometric, and Genetic Integration with Computational intelligence; MASH, metabolic dysfunction-associated steatohepatitis; MASLD, metabolic dysfunction-associated steatotic liver disease; mt-, mitochondria; rsGPT-4, risk score GPT-4.

both biomarkers were included in the MAGIC-Fib, the AUC increased marginally to 73%. These values suggest good discriminative ability, although not substantially different when using both biomarkers *vs.* the *D-loop* alone (Table 3, Fig. 4C). We divided the cohort with MAGIC-Fib quartiles that considers the contribution of *D-loop* alone alongside the co-presence of NRV = 3 to predict the risk of fibrosis: very low-risk (1st quartile: ≤21.83 points), low-risk (2nd quartile: 21.83 to <25.43

points), moderate-risk (3rd quartile: 25.43 to <28.69 points), and high-risk (4th quartile: ≥28.69 points). This division yielded similar findings as above for MAGIC-MASH. Patients in the 4th quartile showed a proportional increased risk of fibrosis compared with patients in the other quartiles (OR 18.43, 95% CI 10.6–32.06, $p$ <0.0001 *vs.* 1st quartile; OR 5.46, 95% CI 3.47–8.58, $p$ <0.0001 *vs.* 2nd quartile; OR 2.56, 95% CI 1.65–3.96, $p$ <0.0001 *vs.* 3rd quartile) (Fig. 4D).

Finally, the most notable increase in prognostic precision was observed in the MAGIC-H score for HCC risk stratification. Here, ccf-COXIII demonstrated a higher AUC than *D-loop* (81% *vs.* 77%, respectively), thus sustaining that ccf-COXIII abundance is a stronger HCC predictor on its own. The dual-biomarkers model reached an AUC of 86% with a sensitivity of 78.6% and specificity of 81.5%, thus optimizing the detection of HCC, particularly at a cut-off risk score set at 30 points (Table 3, Fig. 4E).

To further dissect the predictive power of the MAGIC-H score, we grouped the MASLD cohort into risk score quartiles including both mt-biomarkers (1st quartile: <23.21 points; 2nd quartile: 23.21 to <26.50 points; 3rd quartile: 26.50 to <29.28 points; 4th quartile: ≥29.28 points). At nominal logistic regression analysis, we observed that patients belonging to the 4th quartile showed a significantly increased risk of HCC compared with the 1st (OR 24.37, 95% CI 4.22–184, $p$ = 0.002), 2nd (OR 22.69, 95% CI 3–171, $p$ = 0.002) and 3rd (OR 3.75, 95% CI 1.46–9.62, $p$ = 0.006) quartiles (Fig. 4F). Overall, the use of rsGPT-4 has allowed us to generate new risk models, whose accuracy is weighted on the relative contribution of demographic, genetic, and mt-derived biomarkers.

### Validation of MAGIC scores and comparisons with NITs in Serum Validation/Non-invasive cohorts

In the Serum Validation cohort, we compared established NITs such as Aspartate Aminotransferase to Platelet Ratio Index (APRI), BMI, AST/ALT ratio and diabetes (BARD), BMI, age, ALT, triglycerides (BAAT), Hepatic Steatosis Index (HSI), Forn's index, and Fibrosis score (Fib-4) to our best-performing MAGIC models. Thus, for MASH and fibrosis >1, we used the MAGIC-MASH and MAGIC-Fib calculated with *D-loop* alone, whereas for HCC risk, we used MAGIC-H with both biomarkers. Moreover, we build with RF a transaminase-based score (Score integrating Transaminases, Anthropometric and Genetic Evaluation, STAGE) combining alanine aminotransferase and aspartate aminotransferase with the same anthropometrics and genetic data used for MAGIC scores.

MAGIC-MASH and MAGIC-Fib models showed comparable or slightly superior accuracy relative to NITs, suggesting mt-biomarkers can match traditional approaches for early-stage stratification. Importantly, for HCC risk prediction, the MAGIC-H model consistently outperformed NITs and STAGE and remained the strongest independent predictor of HCC risk even when adjusting for cirrhosis status (Tables S7 and S8).

The validation of MAGIC scores was also performed in an independent cohort of 386 patients with a non-invasive MASLD diagnosis, where fibrosis stage was assessed by FibroScan® (Echosens, Paris, France). In this setting, MAGIC-Fib confirmed its higher predictive value for detecting moderate and advanced fibrosis. Similarly, MAGIC-H maintained robust accuracy for predicting HCC risk, outperforming most existing scores and retaining independent predictive ability even in patients without cirrhosis, a group often missed by traditional NITs (Tables S7 and S8). These results are discussed in the Supplementary material.

## Discussion

Polygenic risk scores (PRS) have gained recognition for MASLD clinical assessment, aiding in identification of patients at high-risk of disease progression, although they face challenges owing to a lack in precision, necessitating compromises in sensitivity/specificity values.[2–4,8,12,17] Previously, we demonstrated the link between the co-presence of *PNPLA3*/*MBOAT7*/*TM6SF2* loss-of-functions and the impairment of mt-flexibility.[8,10,18]

Therefore, the main goals of this study were to investigate the genetic contribution to mt-lifecycle in the liver of patients with MASLD and to find novel biomarkers which may reflect the hepatic mt-alterations, thus providing prognostic approaches for clinical risk assessment. We first characterized the hepatic mt-dynamics and content in a Discovery cohort and the results were replicated in the Hepatic Validation cohort. Secondly, we looked for circulating mt-biomarkers in patients with MASLD, that could be surrogates of hepatic mt-mass and damage.[9,19–22] The choice fell on *D-loop* to assess mt-content in PBMCs, and on ccf-COXIII as a marker of tissue damage measured in serum samples.[9,10,19–22] The potential application of these circulating mt-biomarkers was first assessed in the Serum Validation cohort with histological MASLD diagnosis and then validated in the Non-invasive cohort, who underwent FibroScan®. The accuracy of mt-biomarkers was finally compared with reference NITs and transaminases.

TEM analysis revealed the presence of canonical mt-structures typically giant, swelled, hypodense, and with para-crystalline inclusions. These features have been observed in both MASLD and other types of chronic liver disorders, indicating that such alterations may appear in a non-specific fashion across liver diseases.[23–25] Unexpectedly, a new spectrum of mt-lesions emerged in NRV = 3 carriers from the Discovery cohort, who exhibited the most severe MASLD phenotype. In a case of a 40-year-old woman affected by hypertriglyceridemia and MASLD, non-canonical mt-aberrancies such as *onion-like* mitochondria were identified. These changes were possibly attributable to a range of SNPs implicated in lipid handling, suggesting that alterations in lipid composition may contribute to hepatic mt-morphological changes.[7,8] Likewise, we observed that mt-double-membrane ruptures, irregular cristae arrangements and mt-vacuolization were exclusively detected in NRV = 3 individuals, thus supporting that SNPs in genes regulating hepatic fat metabolism may explain the phenotypic variability in the hepatic mt-architecture compared with the other patients with MASLD with a similar histological degree.

Conflicting results have been reported regarding mt-dynamics in MASLD. Carabelli and collaborators argued that mitobiogenesis increased in high-fat diet-fed rats, whereas Li *et al.* supported that *PGC1-α* and OPA1 overexpression drives tumor growth, invasion, and are associated with poor HCC outcomes.[8,26–28] Conversely, several studies reported

scarce mt-content and *PGC1-α* expression in MASLD.[25] More consistent are data concerning the reduction of PINK/PRKN-dependent mitophagy, responsible for defective mt-accumulation. Here, a significant increase of hepatic mt-number, dimension, and PGC1-α/p38α nuclear translocation was found in NRV = 3 patients. Importantly, the association between genetic background and mt-number was NAS-independent, suggesting a potential link between cumulative genetic risk and altered mt-dynamics leading to increased mt-biomass. Furthermore, high OPA1 and DRP1 levels, involved in mt-fusion and fission, respectively, were observed in NRV = 3 patients, thus accounting for the formation of megamitochondria and the large quantity of mitochondria within liver biopsies. Although hepatic PINK1 was also upregulated in NRV = 3 carriers, PRKN was reduced thus implying that the early arrest of mitophagy cascade may be at the basis of the mt-ultrastructural abnormalities.

Despite our findings partially diverge from previous reports, there are plausible explanations for these discrepancies. Most case studies involve individuals undergoing bariatric surgery, who differ from our cohorts for class enrollment criteria and anthropometric parameters.[13,29] The methodological approach may represent further bias. Compared with Moore *et al*. and Koliaki *et al.*, we assessed protein levels rather than relative gene expression, which provides a direct measure of protein activation.[13,29] Likewise, markers of mt-function (*i.e.* MT-ND1, citrate synthase) rather than direct mt-mass measurements may potentially lead to inaccurate assessment of mt-content[29,30] as mt-function and mass do not always correlate.[31] Notably, our data still indicate an impairment of mt-biogenesis, involving the PGC-1α/p38 pathway which leads to the accumulation of structurally compromised mitochondria.

To deepen the influence of genetics on mt-markers, we correlated TEM and IHC quantifications with the individual *PNPLA3*/*MBOAT7*/*TM6SF2* polymorphisms. Our results showed that the PNPLA3 I148M variant might contribute to the impairment of mt-dynamics without affecting the net mt-content. Instead, the *MBOAT7* and *TM6SF2* mutations unbalanced mt-biogenesis and degradation, thus leading to significant alterations in mt-biomass. These assumptions were supported by multivariate analysis which revealed a strong association among *MBOAT7*/*TM6SF2* SNPs and mt-content.[8,10,18] Despite this study is observational, these findings are consistent with our previous mechanistic work conducted in hepatocyte models, where *PNPLA3*/*MBOAT7*/*TM6SF2* loss-of-function resulted in abnormal mt-biogenesis and structural modifications, through PGC-1α deregulation. Moreover, genetic re-introduction of both *MBOAT7* and *TM6SF2* wild-type forms in the MBOAT7-/-TM6SF2-/- model rescued mt-dynamics and functional impairment, thus supporting the existence of a causal link between genetic risk variants and the mt-alterations found in patients with MASLD.[8,32]

We then aimed to translate our observations into clinical practice by measuring circulating *D-loop* and ccf-COXIII levels in our cohorts, correlating them with both genetics and disease severity with the goal of exploiting them for the development of dynamic risk scores for MASLD monitoring. NRV = 3 carriers showed the highest *D-loop* levels in PBMCs, which positively correlated with hepatic mt-content, indicating that this circulating biomarker reflects the increased mt-mass as in the liver. As these results might suggest that PBMCs increase mt-content in response to hepatic mt-stress, we further investigated potential factors which may promote this mechanism. In the Discovery cohort, we showed the activation of p38 protein, which is involved in the systemic mt-adaptation through the transcription of the GDF15 mitokine.[15,33,34] Therefore, we evaluated its serum levels in 176 patients from the Serum Validation cohort thus revealing an increase of this molecule in NRV = 3 individuals. Moreover, GDF15 correlated with circulating *D-loop*, potentially sustaining that PGC1a/p38/GDF15 cascade may underlie the systemic mt-adaptation.

As concern the impact of the single SNPs on *D-loop* levels, multivariate analysis highlighted that they were independently modulated by *MBOAT7* and *TM6SF2* variants rather than the I148M PNPLA3, reinforcing that these genes might affect mt-dynamism. Moreover, circulating *D-loop* correlated with metabolic comorbidities and progressively increased with hepatic histological damage, supporting its potential as pathological MASLD marker.

Regarding ccf-COXIII, NRV = 3 patients augmented its concentration and, differently from *D-loop*, it associates with all *PNPLA3*/*MBOAT7*/*TM6SF2* SNPs. Thus, despite the I148M PNPLA3 mutation exerts a minor effect on mt-dynamics compared to *MBOAT7* and *TM6SF2* at-risk genotypes, its role stands out most for advanced hepatic injury and possibly mt-dysfunction. Such findings meet confirmation in both *in vitro* models and patients with MASLD, revealing a positive association between the I148M variant and mt-activities (TCA, OXPHOS, β-oxidation).[35,36]

NRV = 3 patients represent the fraction of individuals with the highest disease severity. Accordingly, although ccf-COXIII was not associated with environmental risk factors and MASLD early stages, its release was extremely high in individuals with cirrhosis and HCC, thus representing a potential biomarker for these conditions.

Given the link among genetics, mt-biomarkers and disease progression, the final aim of this work focused on developing non-invasive risk scores integrating genetic information, biochemical parameters, metabolic comorbidities, and mt-derived biomarkers with the purpose to overcome existing challenges.[12] Effective scoring systems for early MASH detection are lacking partly because of the inability of novel biomarkers to predict MASLD progression alone. Thus, new diagnostic/prognostic approaches involve their use in combination and/or with transaminases.[37] PRS have also found their utility for clinical risk stratification in MASLD, but their predictive power alone reaches poor AUC, whereas their incorporation into existing scores for fibrosis and HCC diagnosis, did not significantly improve the predictive accuracy of the models.[17]

Generative AI tools are increasingly used in healthcare particularly for enhancing diagnostic accuracy, treatments, and patient outcomes.[38–40] In recent years, we focused our efforts on meeting the gap related to the impact of the major MASLD-associated genetic variants on disease worsening. Specifically, we attempted to address how: (1) *PNPLA3*/*MBOAT7*/*TM6SF2* SNPs, involved in lipid remodeling, may lead to advanced MASLD forms; and (2) to maximize the use of genetic variants in medical practice by proposing a novel analytical method under AI support.

With rsGPT-4 assistance, we extrapolated defined features (age, BMI, NRV, and the two novel mt-biomarkers) and optimized their combination to obtain robust prediction models ('MAGIC') for MASH, fibrosis, and HCC through machine-learning algorithms. The MAGIC scores differ by the presence of only one or both mt-biomarkers (*D-loop* and/or ccf-COXIII), and the strength of their interactions with at-risk SNPs.

By applying the new scores to the Serum Validation cohort, the MAGIC-MASH and the MAGIC-Fib with *D-loop* alone reached the best AUCs compared with those with ccf-COXIII alone or both biomarkers, with a discrete sensitivity/specificity. Accordingly, the application of the MAGIC-Fib built with *D-loop* in an independent Non-invasive cohort, confirmed its good performance for identifying patients with liver stiffness measurement ≥7 and >10 kPa, supporting that D-loop assessment may be sufficient for the early MASH and fibrosis detection. For HCC, the MAGIC-H generated with ccf-COXIII alone reached a higher AUC than that with *D-loop* (81% *vs.* 77%) and the combination of both biomarkers further improved the model accuracy up to 86%, without restricting sensitivity/specificity parameters (78.6–81.5%) in the Serum Validation cohort. Importantly, MAGIC-H remained independently associated with HCC risk in the multivariable analyses after adjustment for cirrhosis. These findings were confirmed in the Non-invasive cohort, where MAGIC-H with both mt-biomarkers retained its predictive value (AUC: 87%) and associated with HCC risk independently of cirrhosis, thus adding value to this novel tool in the clinical context of non-cirrhotic patients with MASLD, who are not currently included in HCC surveillance.[41]

Finally, we compared the MAGIC scores with established NITs and STAGE in both the Serum Validation/Non-invasive cohorts. In the former, the MAGIC models were superior to APRI, BARD, BAAT, HIS, and Forn's index for HCC monitoring, while they did not yield the statistical significance against Fib-4. In the Non-invasive cohort, the comparisons of MAGIC-H with NITs were less significant. This could be partly attributed to the fact that all HCC individuals in this cohort had cirrhosis, which conventional NITs are specifically designed to capture.

Regarding the comparison with STAGE, our data indicates that both *D-loop* and ccf-COXIII are good proxies of liver disease progression, showing similar rates to canonical markers of hepatic injury. Nonetheless, mt-biomarkers were superior to transaminases for the identification of MASLD-HCC cases in both Serum Validation/Non-invasive cohorts, potentially adding a new non-invasive tool to predict patient prognosis.

In conclusion, new hits emerged from this study. First, mounting evidence indicates that genetics cannot be thought of as a marginal part of pathology. The I148M PNPLA3 variant affects hepatic functions whereas *MBOAT7/TM6SF2* SNPs impact on mt-biogenesis possibly through changes in lipid species. The study dissected the role of two novel mt-biomarkers: *D-loop* resulted highly informative for earlier MASLD stages, whereas ccf-COXIII closely correlated with the worst MASLD forms. Both mt-biomarkers increased in individuals with HCC and their combination in the MAGIC-H score provided the best prognostic performance. We recognized that developing new risk scores with AI can be challenging and necessitate future validations. Nevertheless, it helped to optimize the use of genetic data and circulating biomarkers, while considering the causal relationship between them, enabling the generation of scores with an AUC comparable and/or superior to the existing ones for MASLD-HCC monitoring.

**Affiliations**

[1]*Medicine and Metabolic Diseases, Fondazione IRCCS Cà Granda Ospedale Maggiore Policlinico, Milan, Italy;* [2]*Neuromuscular and Rare Diseases Unit, Department of Neuroscience, Fondazione IRCCS Ca' Granda Ospedale Maggiore Policlinico, Milan, Italy;* [3]*Biology of Myelin Unit, Division of Genetics and Cell Biology, IRCCS San Raffaele Scientific Institute, Milan, Italy;* [4]*Department of Pathophysiology and Transplantation, Università Degli Studi di Milano, Milan, Italy;* [5]*Clinical Pathology, Fondazione IRCCS Ca' Granda Ospedale Maggiore Policlinico, Milan, Italy;* [6]*Division of Pathology, Fondazione IRCCS Ca' Granda Ospedale Maggiore Policlinico, Milan, Italy;* [7]*Research Unit of Genetics of Complex Phenotypes, "Bambino Gesù" Children's Hospital, IRCCS, Rome, Italy;* [8]*Department of Translational Medicine and Surgery, Catholic University, Fondazione Policlinico Universitario A. Gemelli IRCCS, Rome, Italy;* [9]*CEMAD Unit, Digestive Disease Center, Fondazione Policlinico Universitario A. Gemelli IRCCS, Rome, Italy;* [10]*Department of Medical Area (DAME), University of Udine and Italian Liver Foundation, Bldg Q AREA Science Park - Basovizza Campus, Trieste, Italy*

## Abbreviations

AI, artificial intelligence; ccf, cell-free circulating; DRP1, Dynamin-related protein 1; GDF15, growth differentiation factor 15; GLM, generalized linear model; GM, giant mitochondria; HCC, hepatocellular carcinoma; IHC, immunohistochemistry; LDs, lipid droplets; MAGIC, Mitochondrial, Anthropometric, and Genetic Integration with Computational intelligence; MASH, metabolic dysfunction-associated steatohepatitis; MASLD, metabolic dysfunction-associated steatotic liver disease; mt-, mitochondria; NAS, Non-alcoholic fatty liver disease Activity Score; NITs, non-invasive tests; NRV, number of risk variants; OPA1, mt-dynamin-like GTPase; OR, odds ratio; PBMCs, peripheral blood mononuclear cells; *PGC-1α*, *peroxisome proliferator-activated receptor-gamma coactivator*; PRKN, Parkin; PRS, polygenic risk scores; RF, random forest; rsGPT-4, risk score GPT-4; SNPs, single nucleotide polymorphisms; STAGE, Score integrating Transaminases, Anthropometric and Genetic Evaluation; TEM, transmission electron microscopy.

## Financial support

This study was supported by Italian Ministry of Health (Ricerca Corrente 2024 - Fondazione IRCCS Cà Granda Ospedale Maggiore Policlinico), by the Italian Ministry of Health (Ricerca Finalizzata Ministero della Salute GR-2019-12370172; RF-2021-12374481) and by 5x1000 2020 RC5100020B; Bando Ricerca Corrente and Piano Nazionale Complementare Ecosistema Innovativo della Salute - Hub Life Science-Diagnostica Avanzata (HLS-DA) - PNC-E3-2022-23683266 - 'INNOVA'. The Department of Pathophysiology and Transplantation, University of Milan, is funded by the Italian Ministry of Education and Research (MUR): Dipartimenti di Eccellenza Program 2023 to 2027).

## Conflicts of interest

The authors declare that they have no conflicts of interest.

Please refer to the accompanying ICMJE disclosure forms for further details.

## Authors' contributions

Study design: ML, PD. Conceptualization of analysis by AI tool: ML. Acquisition of TEM images: MR, LN. Statistical analysis and support in managing AI tool: FG. Patient recruitment: AC, MMa, AA, LM, AL, GS, AG. Data collection: AC, MMa, AA, LM, AL, GS, AG, ALF. Data analysis: ML, EP, MMe. Data interpretation: ML, EP, MMe, MMo. Manuscript drafting: ML, PD. Manuscript revision: ALF. Funding acquisition, supervision, and primary responsibility for final content: PD. Read and approved the final manuscript: all authors.

## Data availability

Further information and requests for resources, reagents and data should be directed to, and will be fulfilled by, the lead contact, PD (paola.dongiovanni@policlinico.mi.it).

## Acknowledgements

AA is supported by Italian Ministry of Health with “Current Research funds”.

## Supplementary data

Supplementary data to this article can be found online at https://doi.org/10.1016/j.jhepr.2025.101539.

## References

*Author names in bold designate shared co-first authorship*

[1] Younossi ZM, Golabi P, Paik JM, et al. The global epidemiology of nonalcoholic fatty liver disease (NAFLD) and nonalcoholic steatohepatitis (NASH): a systematic review. Hepatology 2023;77:1335–1347.
[2] **Bianco C**, **Jamialahmadi O**, **Pelusi S**, et al. Non-invasive stratification of hepatocellular carcinoma risk in non-alcoholic fatty liver using polygenic risk scores. J Hepatol 2021;74:775–782.
[3] **Dongiovanni P**, **Petta S**, Maglio C, et al. Transmembrane 6 superfamily member 2 gene variant disentangles nonalcoholic steatohepatitis from cardiovascular disease. Hepatology 2015;61:506–514.
[4] **Mancina RM**, **Dongiovanni P**, Petta S, et al. The MBOAT7-TMC4 variant rs641738 increases risk of nonalcoholic fatty liver disease in individuals of European descent. Gastroenterology 2016;150:1219–1230.e1216.
[5] Calamita G, Gena P, Meleleo D, et al. Water permeability of rat liver mitochondria: a biophysical study. Biochim Biophys Acta 2006;1758:1018–1024.
[6] Szendroedi J, Phielix E, Roden M. The role of mitochondria in insulin resistance and type 2 diabetes mellitus. Nat Rev Endocrinol 2012;8:92–103.
[7] **Meroni M**, **Longo M**, Paolini E, et al. Expanding the phenotypic spectrum of non-alcoholic fatty liver disease and hypertriglyceridemia. Front Nutr 2022;9:967899.
[8] **Longo M**, **Meroni M**, Paolini E, et al. TM6SF2/PNPLA3/MBOAT7 loss-of-function genetic variants impact on NAFLD development and progression both in patients and in in vitro models. Cell Mol Gastroenterol Hepatol 2022;13:759–788.
[9] Ma C, Liu Y, He S, et al. Association between leukocyte mitochondrial DNA copy number and non-alcoholic fatty liver disease in a Chinese Population is mediated by 8-oxo-2’-deoxyguanosine. Front Med 2020;7:536.
[10] Paolini E, Longo M, Corsini A, et al. The non-invasive assessment of circulating D-Loop and mt-ccf levels opens an intriguing spyhole into novel approaches for the tricky diagnosis of NASH. Int J Mol Sci 2023;24:2331.
[11] **Longo M**, **Paolini E**, Meroni M, et al. Remodeling of mitochondrial plasticity: the key switch from NAFLD/NASH to HCC. Int J Mol Sci 2021;22:4173.
[12] Singh SP, Barik RK. Noninvasive biomarkers in nonalcoholic fatty liver disease: are we there yet? J Clin Exp Hepatol 2020;10:88–98.
[13] Moore MP, Cunningham RP, Meers GM, et al. Compromised hepatic mitochondrial fatty acid oxidation and reduced markers of mitochondrial turnover in human NAFLD. Hepatology 2022;76:1452–1465.
[14] Aharoni-Simon M, Hann-Obercyger M, Pen S, et al. Fatty liver is associated with impaired activity of PPARγ-coactivator 1α (PGC1α) and mitochondrial biogenesis in mice. Lab Invest 2011;91:1018–1028.
[15] Shimizu S, Kadowaki M, Yoshioka H, et al. Proteasome inhibitor MG132 induces NAG-1/GDF15 expression through the p38 MAPK pathway in glioblastoma cells. Biochem Biophys Res Commun 2013;430:1277–1282.
[16] Takeuchi K, Yamaguchi K, Takahashi Y, et al. Hepatocyte-specific GDF15 overexpression improves high-fat diet-induced obesity and hepatic steatosis in mice via hepatic FGF21 induction. Sci Rep 2024;14:23993.
[17] EASL-EASD-EASO Clinical Practice Guidelines for the management of nonalcoholic fatty liver disease. J Hepatol 2016;64:1388–1402.
[18] Meroni M, Dongiovanni P, Longo M, et al. Mboat7 down-regulation by hyper-insulinemia induces fat accumulation in hepatocytes. EBioMedicine 2020;52:102658.
[19] Weng SW, Lin TK, Liou CW, et al. Peripheral blood mitochondrial DNA content and dysregulation of glucose metabolism. Diabetes Res Clin Pract 2009;83:94–99.
[20] Malik AN, Shahni R, Iqbal MM. Increased peripheral blood mitochondrial DNA in type 2 diabetic patients with nephropathy. Diabetes Res Clin Pract 2009;86:e22–e24.
[21] Garcia-Martinez I, Santoro N, Chen Y, et al. Hepatocyte mitochondrial DNA drives nonalcoholic steatohepatitis by activation of TLR9. J Clin Invest 2016;126:859–864.
[22] Zhou G, Li Y, Li S, et al. Circulating cell-free mtDNA content as a non-invasive prognostic biomarker in HCC patients receiving TACE and traditional Chinese medicine. Front Genet 2021;12:719451.
[23] Shami GJ, Cheng D, Verhaegh P, et al. Three-dimensional ultrastructure of giant mitochondria in human non-alcoholic fatty liver disease. Sci Rep 2021;11:3319.
[24] Ma X, Chen A, Melo L, et al. Loss of hepatic DRP1 exacerbates alcoholic hepatitis by inducing megamitochondria and mitochondrial maladaptation. Hepatology 2023;77:159–175.
[25] Ahishali E, Demir K, Ahishali B, et al. Electron microscopic findings in non-alcoholic fatty liver disease: is there a difference between hepatosteatosis and steatohepatitis? J Gastroenterol Hepatol 2010;25:619–626.
[26] Carabelli J, Burgueño AL, Rosselli MS, et al. High fat diet-induced liver steatosis promotes an increase in liver mitochondrial biogenesis in response to hypoxia. J Cell Mol Med 2011;15:1329–1338.
[27] Li Y, Xu S, Li J, et al. SIRT1 facilitates hepatocellular carcinoma metastasis by promoting PGC-1α-mediated mitochondrial biogenesis. Oncotarget 2016;7:29255–29274.
[28] Li M, Wang L, Wang Y, et al. Mitochondrial fusion via OPA1 and MFN1 supports liver tumor cell metabolism and growth. Cells 2020;9:121.
[29] Koliaki C, Szendroedi J, Kaul K, et al. Adaptation of hepatic mitochondrial function in humans with non-alcoholic fatty liver is lost in steatohepatitis. Cell Metab 2015;21:739–746.
[30] Castellani CA, Longchamps RJ, Sun J, et al. Thinking outside the nucleus: mitochondrial DNA copy number in health and disease. Mitochondrion 2020;53:214–223.
[31] Wredenberg A, Wibom R, Wilhelmsson H, et al. Increased mitochondrial mass in mitochondrial myopathy mice. Proc Natl Acad Sci U S A 2002;99:15066–15071.
[32] Paolini E, Longo M, Meroni M, et al. A defective circulating mitochondrial bioenergetics profile reflects the hepatic one and outlines genetic MASLD. Antioxidants 2025;14:618.
[33] Jena J, García-Peña LM, Pereira RO. The roles of FGF21 and GDF15 in mediating the mitochondrial integrated stress response. Front Endocrinol 2023;14:1264530.
[34] Zhang B, Chang JY, Lee MH, et al. Mitochondrial stress and mitokines: therapeutic perspectives for the treatment of metabolic diseases. Diabetes Metab J 2024;48:1–18.
[35] Caon E, Martins M, Hodgetts H, et al. Exploring the impact of the PNPLA3 I148M variant on primary human hepatic stellate cells using 3D extracellular matrix models. J Hepatol 2024;80:941–956.
[36] Luukkonen PK, Porthan K, Ahlholm N, et al. The PNPLA3 I148M variant increases ketogenesis and decreases hepatic de novo lipogenesis and mitochondrial function in humans. Cell Metab 2023;35:1887–1896.e1885.
[37] Shen J, Chan HL, Wong GL, et al. Non-invasive diagnosis of non-alcoholic steatohepatitis by combined serum biomarkers. J Hepatol 2012;56:1363–1370.
[38] Nam D, Chapiro J, Paradis V, et al. Artificial intelligence in liver diseases: improving diagnostics, prognostics and response prediction. JHEP Rep 2022;4:100443.
[39] Yim D, Khuntia J, Parameswaran V, et al. Preliminary evidence of the use of generative AI in health care clinical services: systematic narrative review. JMIR Med Inform 2024;12:e52073.
[40] Rodriguez DV, Lawrence K, Gonzalez J, et al. Leveraging generative AI tools to support the development of digital solutions in health care research: case study. JMIR Hum Factors 2024;11:e52885.
[41] EASL Clinical Practice Guidelines on the management of hepatocellular carcinoma. J Hepatol 2025;82:315–374.

Keywords: Non-invasive scores; mtDNA; *PNPLA3*/*MBOAT7*/*TM6SF2*; GPT-4; MASLD-HCC.
*Received 8 November 2024; received in revised form 22 July 2025; accepted 24 July 2025; Available online 31 July 2025*